CHAPTER 4

Adaptive Streamflow Rating Curve Estimation: AdaptRatin

4.1 Abstract

Water resource management is impossible without accurate information about stream discharge. However measuring stream discharge is difficult and therefore stage height measurements, which are easier to obtain, are used as proxies. The conversion of stage height to stream discharge relies on a stage-discharge relationship, which is unique to individual gauging station and is known as a 'rating curve'. Accurate assessment of this rating curve, and accompanying predictions, is essential for effective water resources management. The stage-discharge relationship can be non-stationary, due to erosion or sediment deposition at gauging sites which results from natural processes such as flooding. As a result, the rating curve needs to be re-calibrated regularly. This chapter presents an approach to estimate the time-varying stage-discharge relationships, referred to as Adaptive Streamflow Rating Curve Estimation (AdaptRatin). The proposed AdaptRatin algorithm first partitions the time-ordered data into an unknown yet finite number of locally stationary segments. Within each segment, the stage-discharge relationship is modelled non-parametrically by placing a *Gaussian process* prior over the unknown relationship. A Bayesian approach is used for the inference of the number and location of locally stationary segments as well as their corresponding rating curves via the joint posterior distribution. *Reversible Jump Markov Chain Monte Carlo* (RJMCMC) is used to obtain a sample-based estimate of this joint posterior. It is shown that AdaptRatin can successfully capture the changes in the stage-discharge relationship over time and provide reliable estimates of the underlying stage-discharge relationship for each time period for both stationary and non-stationary processes is demonstrated.

4.2 Introduction

Stream discharge (volume per unit time) is a fundamental variable in hydrology and plays a crucial role in water resource management. However, continuous direct measurement of stream discharge is challenging as it generally involves labor-intensive and expensive procedures as explained in chapter 1 section 1.3. Often stream discharge is calculated by converting more easily obtained continuous stream height measurements via a stage-discharge relationship formally known in hydrology as a 'rating curve' (ISO, 2010; Organization, 2010). In practise, only limited concurrent direct measurements of both stage height and stream discharge are taken at a gauging station to build the stage-discharge relationship. Accurately quantifying the uncertainty associated with the rating curve is imperative for making informed decisions in water resource management, as the rating curve serves as the foundation for various hydrological analyses based on stream discharge, including hydrological model calibration (Westerberg et al., 2022), flood forecasting (Ocio et al., 2017), and water accounting (Lowe et al., 2009).

A study by McMahon and Peel (2019), which assessed the accuracy of rating curves for 171 Australian Bureau of Meteorology Hydrologic reference stations, reported that levels of uncertainty in streamflows predicted using the rating curve ranged from +29% to -22%, and this uncertainty needs to be factored into any decisions which are reliant on these predictions.

In natural river settings, the stage-discharge relationship can change due to many factors that influence the cross-sectional area of the river at the gauging site, such as erosion, sediment deposition and vegetation growth (Mansanarez et al., 2019). To model these temporal variations and to quantify the uncertainty of their associated rating curves, existing methods typically fall into two categories (Darienzo et al., 2021):

(1) Methods which account for gradual transient changes in the rating curve relationship (Morlot et al., 2014; Reitan and Petersen-Overleir, 2009; Perret et al., 2021).
(2) Methods which account for sudden changes in the rating curve relationship (Mansanarez et al., 2019; Qiu et al., 2021; Darienzo et al., 2021)

This study is an example of the second approach, considering that 70% of rivers in Australia are ephemeral, with sediment transportation being episodic and event-driven. Consequently, changes to the cross-sectional area are more likely to be sudden rather than gradual.

The most commonly used technique in determining changes in the rating curve, which are the result of sudden changes in the cross sectional area, involves the use of predefined empirical threshold values. When measured discharge values deviate beyond these thresholds from the discharge calculated using the current rating curve, the rating curve's validity is deemed compromised (Organization, 2010). For example, in the United States, a departure of a discharge measurement from a defined rating curve beyond $\pm 5\%$ of the discharge value is defined as the threshold. In practical scenarios, such approaches are easy to implement but may not be reliable for all stations across different hydro-geological conditions.

Several other data-driven statistical methods have been proposed to identify sudden changes in the rating curve. The simplest approach is by Van Eerdenbrugh et al. (2017), who propose a consistency assessment method that relies on identifying systematic deviations in the gaugings, beyond a certain threshold value (based on regional information) from the current rating curve relationship. This method is very similar to the empirical threshold value method explained before (Organization, 2010) except for the use of regional information in defining station specific threshold values. Qiu et al. (2021) propose a two-step procedure to estimate non-stationary rating curves. First, the gauging data is divided into homogeneous groups based on the mean of the residuals, using a multiple change point detection algorithm. Next, the stationary rating curves in the homogeneous groups are calibrated using the BaRatin method (Le Coz et al., 2014). For a single station with a large amount of hydraulic information on the topology of the cross-section, this approach works well, however, the suitability of the method for stations with minimal prior information is difficult to assess. Furthermore, this method cannot quantify the uncertainty of the estimated change point. Darienzo et al. (2021) has proposed a recursive segmentation procedure based on residuals to identify shifts in rating curves and has used the BaRatin method to estimate the rating curve for each segment. This method also relies on hydraulic information for the gauging station and assumes that the standard deviation of the residuals for each stationary segment of the rating curve

is known apriori before implementing the segmentation. This means that the resulting segmentation of the gauging data for each iteration of the proposed recursive algorithm may depend on the assigned standard deviations and lead to varying results for different values of standard deviations assigned by the user. Since the primary objective of the procedure is to identify changes in the rating curve, relying on user-defined values to identify a shift rather than the gauging data itself could introduce significant bias into the results. Nevertheless, all these methodologies provide useful insights on how the problem of non-stationary rating curves can be approached.

The main objective of this chapter is to propose a data-driven methodology to estimate the non-stationary rating curves which can;

(1) Identify changes in the rating curve and quantify the uncertainty in the estimated change points.
(2) Estimate the rating curve for each identified stationary period.
(3) As a check on the method, estimate the rating curve for cases when the rating curve does not change (the rating curve is stationary).

This chapter follows the method outlined in Rosen et al. (2012) to divide the time series into an unknown yet finite number of segments. Within each segment the dependency between measured stream height and discharge is modelled by placing a Gaussian process prior over the unknown relationship.

The structure of the chapter is as follows. Section 4.3 introduces the model proposed for estimating non-stationary rating curves. Section 4.4 presents the priors used for data segmentation and the rating curve parameters. Section 4.5 describes the Bayesian inference of the model. Section 4.6 introduces the data used in this study for both simulated data and the real data. The results using AdaptRatin are given in section 4.7 followed by the discussion in section 4.8. Finally, the conclusion of the chapter is given in section 4.9.

4.3 Model

4.3.1 Notation

Let n gauging measurements, $\mathcal{G} := \langle t_1, \tilde{h_1}, \tilde{q_1}\rangle, \ldots, \langle t_n, \tilde{h_n}, \tilde{q_n}\rangle$, take place at a particular station where for $i \in \{1, \ldots, n\}$, the i-th gauging, $\langle t_i, \tilde{h_i}, \tilde{q_i}\rangle$, is a tuple of *measurement time*, t_i, *measured stage height*, $\tilde{h_i}$, and the corresponding *measured stream discharge*, $\tilde{q_i}$.

The measurements are assumed to be in chronological order. That is, for any $i, j \in \{1, \ldots, n\}$, if $i < j$ then $t_i < t_j$. Nonetheless, there is no restriction on the time interval between the consecutive measurements. That is $t_{i+1} - t_i$ can be any positive number.

The vector of all measured stream discharges is denoted by $\tilde{\mathbf{q}} := (\tilde{q_1}, \ldots, \tilde{q_n})'$ and $\tilde{\mathbf{h}} := (\tilde{h_1}, \ldots, \tilde{h_n})'$ represent all measured stage heights. The units of stream discharge and stage height values used throughout this chapter are cubic meters per second (cumec) and meters (m) respectively.

4.3.2 Stage-discharge relationship

The most commonly used relationship for the rating curve in hydrology is the power law relationship of the form;

$$\tilde{q_t} := a(\tilde{h_t} - c)^b, \tag{4.1}$$

where c is the gauge height at zero stream discharge, a and b are parameters related to the cross section of the gauging station.

Although this relationship has been widely used in practice and appears in standards related to the formulation of the stage-discharge relationship (Grant and Paul, 2019), it is an over-simplification of the real hydraulics at many gauging stations (Fenton, 2018). In this chapter, the stage-discharge relationship is modelled non-parameterically by placing a *Gaussian process* prior (see (Neal, 1999) for a detailed theoretical explanation of Gaussian process priors)

over the unknown relationship which is smooth but flexible enough to estimate a large range of possible functions. This method is explained in detail in the next sub-section.

4.3.3 Gaussian process prior over the unknown stage-discharge relationship

The log space is used for both stage height and discharge variables, and thus $y_i := \log(\tilde{q_i})$ and $h_i := \log(\tilde{h_i})$ are defined. The stage-discharge relationship is then formulated between log stage height and log discharge as;

$$y_i = g\left(h_i\right) + \epsilon_i, \text{ where } \epsilon_i \sim \mathcal{N}(0, \sigma^2) \tag{4.2}$$

A prior for g is chosen to ensure the estimate of g is smooth yet flexible enough to accommodate a large range of possible functions. To achieve this, the function is decomposed into two components following Wood (2013), so that:

$$g\left(h_i\right) = \alpha_0 + \alpha_1 h_i + f(h_i) \tag{4.3}$$

and $\boldsymbol{\alpha} := (\alpha_0, \alpha_1)'$

Let $\mathbf{X} := (\mathbf{1}_n, \mathbf{h})$ be the $n \times 2$ *design matrix*, where $\mathbf{1}_n$ is an n-vector of ones and $\mathbf{h} := (h_i, \ldots, h_n)$. The i-th row of $\mathbf{X}$ is denoted as $\mathbf{x}_i$. That is, $\mathbf{x}_i := (1, h_i)$ and $\mathbf{X} := (\mathbf{x}_1, \ldots, \mathbf{x}_n)'$. Then (4.3) can be written as;

$$g\left(h_i\right) = \mathbf{x}_i\boldsymbol{\alpha} + f(h_i)$$

An integrated Wiener process prior (Wahba, 1990) is placed over the function f, so that;

$$f \sim \mathcal{GP}(0, \tau^2\Omega), \tag{4.4}$$

where $\tau^2\mathbf{\Omega}$ is the covariance matrix.

The prior in (4.4) is for a continuous function. Any subset of the function, f, denoted by, $\mathbf{f} := (f(h_1), \ldots, f(h_n))$ then has a multivariate-normal distribution,

$$\mathbf{f} \sim \mathcal{MVN}(0, \tau^2\mathbf{\Omega}_n), \tag{4.5}$$

where $\omega_{u,v} := \text{cov}(f(h_u), f(h_v))$ is the $(u, v)^{th}$ element of $\mathbf{\Omega}_n$ (Wahba, 1990), with

$$\omega_{u,v} := h_u^2(h_v - h_u/3)/2, \text{ for } (h_u \leq h_v)$$

τ^2 is a smoothing parameter and controls the wiggliness of the estimated function. If $\tau^2 = 0$, then the estimate of $f(h_i)$ reduces to the linear component $\mathbf{x}_i\boldsymbol{\alpha}$, and as $\tau^2 \to \infty, \mathbb{E}(f(h_i)|\mathbf{y}) \to y_i$

The prior in (4.5) is reformulated as follows;

Let $\mathbf{\Omega}_n := \mathbf{V}_n\boldsymbol{\lambda}_n\mathbf{V}_n'$ be the eigenvalue decomposition of $\mathbf{\Omega}$, and let $\boldsymbol{\beta}^* \sim \mathcal{MVN}(0, \tau^2\boldsymbol{\lambda}_n)$, then;

$$\mathbf{f} := \mathbf{V}_n\boldsymbol{\beta}^* \sim \mathcal{MVN}(0, \tau^2\mathbf{\Omega}_n) \tag{4.6}$$

The advantage of defining the unknown non-linear function as a linear combination of basis functions in Equation 4.6 is that it results in the model in Equation 4.2 being linear in the unknown parameters $\boldsymbol{\alpha}$ and $\boldsymbol{\beta}^*$,

$$y_i = \mathbf{x}_i\boldsymbol{\alpha} + \mathbf{v}_i\boldsymbol{\beta}^* + \epsilon_i,$$

where $\mathbf{v}_i$ is the i-th row of $\mathbf{V}_n$.

In cases where n is large, eigenvalue decomposition of $\boldsymbol{\Omega}_n$ and estimating $\boldsymbol{\beta}^*$ is computationally infeasible. In this study, it is assumed that retaining only the basis functions corresponding to the top 5 eigenvalues is sufficient to capture deviations from the first-degree polynomial and this significantly enhances the computational efficiency of the proposed AdaptRatin method.

4.3.4 Non-stationarity over time

The stage-discharge relationship can change over time as a result of the changes in the cross sectional area of the river (as explained in section 4.2). Let m be the number of such different stage-discharge relationships in a given record of gauging data. Let $\xi_{j,m}$ be the corresponding i when the validity of the j^{th} stage-discharge relationship end, $j = 1, \ldots, m$ where $\xi_{0,m}$ and $\xi_{m,m}$ are $i = 0$ and $i = n$, so that,

$\mathbf{y}^{[j]} := \{y_i : \xi_{(j-1),m} < i \leq \xi_{j,m}\}$
$\mathbf{h}^{[j]} := \{h_i : \xi_{(j-1),m} < i \leq \xi_{j,m}\}$

$$\mathbf{y} := (\mathbf{y}^{[1]}, \ldots, \mathbf{y}^{[m]})$$
$$\mathbf{h} := (\mathbf{h}^{[1]}, \ldots, \mathbf{h}^{[m]})$$

Conditional on the partition, $\boldsymbol{\xi}_m := (\xi_{0,m}, \ldots, \xi_{m,m})$, the smoothing parameter vector, $\boldsymbol{\tau}_m^2 := (\tau_1^2, \ldots, \tau_m^2)$, log stage height measurements, $\mathbf{h}$, and the rating curve parameter vector, $\boldsymbol{\theta}_m := (\boldsymbol{\theta}^{[1]}, \ldots, \boldsymbol{\theta}^{[j]}, \ldots, \boldsymbol{\theta}^{[m]})$, $\boldsymbol{\theta}^{[j]} := (\boldsymbol{\alpha}_j', \boldsymbol{\beta}_j', \boldsymbol{\sigma}_j^2)$, the likelihood of log discharge, $\mathbf{y}$, is,

$$\mathcal{L}(\mathbf{y}|\mathbf{h},\boldsymbol{\theta},\boldsymbol{\xi}_m,\boldsymbol{\tau}_m^2) = \prod_{j=1}^{m}(2\pi\sigma_j^2)^{-n_j/2} \prod_{i=\xi_{(j-1),m}}^{i=\xi_{j,m}} \exp\left\{-\frac{1}{2}\left(\frac{y_i-(\mathbf{x}_i\boldsymbol{\alpha}_j+\mathbf{v}_i\boldsymbol{\beta}_j)}{\sigma_j}\right)^2\right\},$$

where n_j is the number of data points in segment j. β_j is the vector of regression coefficients for the 5 basis function retained for segment j

4.4 Priors

The parameter vector for AdaptRatin is $\boldsymbol{\Psi} := (\boldsymbol{\theta}_m, \boldsymbol{\tau}_m^2, \boldsymbol{\xi}_m)$. The specific priors placed on each of the parameters are given in the next sub-sections.

4.4.1 Priors on the number of partitions m and the partition $\boldsymbol{\xi}_m$

The prior distribution on the number of segments m is modeled as a discrete uniform distribution, denoted as $m \sim \mathcal{U}(m_{\text{min}}, m_{\text{max}})$, where m_{min} and m_{max} represents the minimum and maximum allowable number of segments respectively. Specifically, the probability of m taking on any particular value k within the range m_{min} to m_{max} is uniform, given by,

$$Pr(m = k|m_{\text{min}}, m_{\text{max}}) = 1/(m_{\text{max}} - m_{\text{min}+1})$$

Typically, m_{min} is set to 1 and m_{max} is set to a value large enough to encompass all identifiable segments. However, if upon executing the procedure, the probability $Pr(m = m_{\text{max}})$ is not approximately zero, indicating potential underestimation of the required number of segments, then m_{max} is increased.

Given the number of segments m, the prior on the partition ξ_m is:

$$Pr(\xi_m|m) = \frac{1}{{}_{n_r+m-1}C_{m-1}},$$

where $n_r := n - (m \times i_{\text{min}})$, is the remaining number of data points left after allocating the minimum number of data points to generate a valid segmentation from n data points. i_{min} is the minimum number of gaugings required for a valid segment.

The notation ${}^{n}C_k := \frac{n!}{k!(n-k)!}$. ${}_{n_r+m-1}C_{m-1}$ gives the number of possible ways to distribute the remaining n_r data points among the m segments.

Then the probability of a specific segmentation ξ_m is given by,

$$Pr(\xi_m, m) = Pr(m = k|m_{\text{min}}, m_{\text{max}}) \times Pr(\xi_m|m = k)$$

4.4.2 Priors on the rating curve parameters and the smoothing parameter

An inverse-gamma prior is placed on σ^2,

$$\sigma^2 \sim \mathcal{IG}(u_0, v_0),$$

The shape and rate parameters of the inverse-gamma prior are set to $u_0 = v_0 = 0.001$ to ensure it remains non-informative (Gilks et al., 1994; Gelman, 2006). The prior on the smoothing parameter τ^2 is also inverse-gamma with the same shape and rate parameters $a_0 = b_0 = 0.001$,

$$\tau^2 \sim \mathcal{IG}(a_0, b_0)$$

A multivariate-normal prior is placed on $\boldsymbol{\alpha}$,

$$\boldsymbol{\alpha} \sim \mathcal{MVN}(0, c_{\alpha}\mathbf{I}_2)$$

To reflect the limited prior knowledge on the relevant linear relationship between h_i and y_i, the c_α parameter of the multivariate-normal prior on α is set to the number of gaugings available, n.

The selection of these specific priors also facilitates the formulation of effective proposal distributions for each parameter in the Metropolis-Hastings algorithm, which is crucial for the overall sampling process described in section 4.5. Given a segmentation ξ, the conditional posterior distributions of each parameter $\boldsymbol{\alpha}, \boldsymbol{\beta}, \sigma^2$, and τ^2 have a closed form, and these are used as proposal distributions in the sampling scheme. The derived conditional posterior distributions of these parameters are given in the Appendix D.

The final step of specifying the priors involves imposing the underlying physical constraint of a stage-discharge relationship, which must be monotonically increasing (since the discharge cannot decrease with increasing stage height). This prior knowledge is imposed on each stationary segment as;

$$p(g(\mathbf{h}|\boldsymbol{\alpha}, \boldsymbol{\beta})) = \begin{cases} 1 & \text{if } g(\mathbf{h}|\boldsymbol{\alpha}, \boldsymbol{\beta}) \text{ is monotonically increasing} \\ 0 & \text{otherwise} \end{cases}$$

4.5 Bayesian Inference

The procedure described in AdaptSPEC (Rosen et al., 2012) is utilized to partition the time series into an unknown yet finite number of segments. The relationship between the log stage height and log stream discharge within each segment is modelled by placing a *Gaussian process prior* as explained in section 4.3.3.

AdaptSPEC contains two types of moves;

(1) Within-model moves: Given the current number of segments m^c, a single partition point ξ_{k^*,m^c} is proposed, where k^* is the chosen segment to be changed. The rating curve parameters of the adjacent segments affected by the relocation are then updated. The proposed rating curves are evaluated for monotonic increase and the two steps are then jointly accepted or rejected in a Metropolis-Hastings step. The smoothing parameters are then updated in a Gibbs step.

(2) Between-model moves: Number of segments are proposed to either increase (birth) or decrease (death) by one. The rating curve parameters of the newly created or removed segments are then updated. The proposed rating curves are evaluated for monotonic increase and the two steps are then jointly accepted or rejected in a Metropolis-Hastings step.

Three chains with different initiation points were run to draw 100000 samples for each data set. The first 50000 samples were discarded and the remaining 50000 samples were used in the inference. The time taken to draw 50000 samples for the Carroll Gap station dataset (214 gaugings) was around 30 minutes using a single CPU.

See Appendix E for a detailed explanation of the sampling algorithm.

4.6 Data

The methodology is demonstrated using data from four gauging stations in Australia which have distinct rating curve shapes as shown in Figure 4.1. The station information and the relevant time periods used for each station along with the number of gaugings used for the study are given in Table 4.1.

TABLE 4.1. Streamflow gauging stations used in the study

River	Station name	station ID	Data from	Number of gaugings
Peel river	Carrol Gap	419006	2000/1/31	214
Lerderderg river	Sardine Creek at O'Brien crossing	231213A	2000/1/1	137
William river	Tillegra	210011	2005/1/1	73
Namoi	North Cuerindi	419005	1950/1/1	132

Gauging data available for all the stations from the starting dates given in Table 4.1 until 2023/1/1 were considered in the study except for the North Cuerindi station in Namoi river which was used for the simulation study. The specific gauging periods used for each simulation study are given in the sections 4.7.1.1 and 4.7.1.2. The reason to select a shorter period of time for Tillegra station is to test the performance of AdaptRatin when there are limited number of gaugings available.

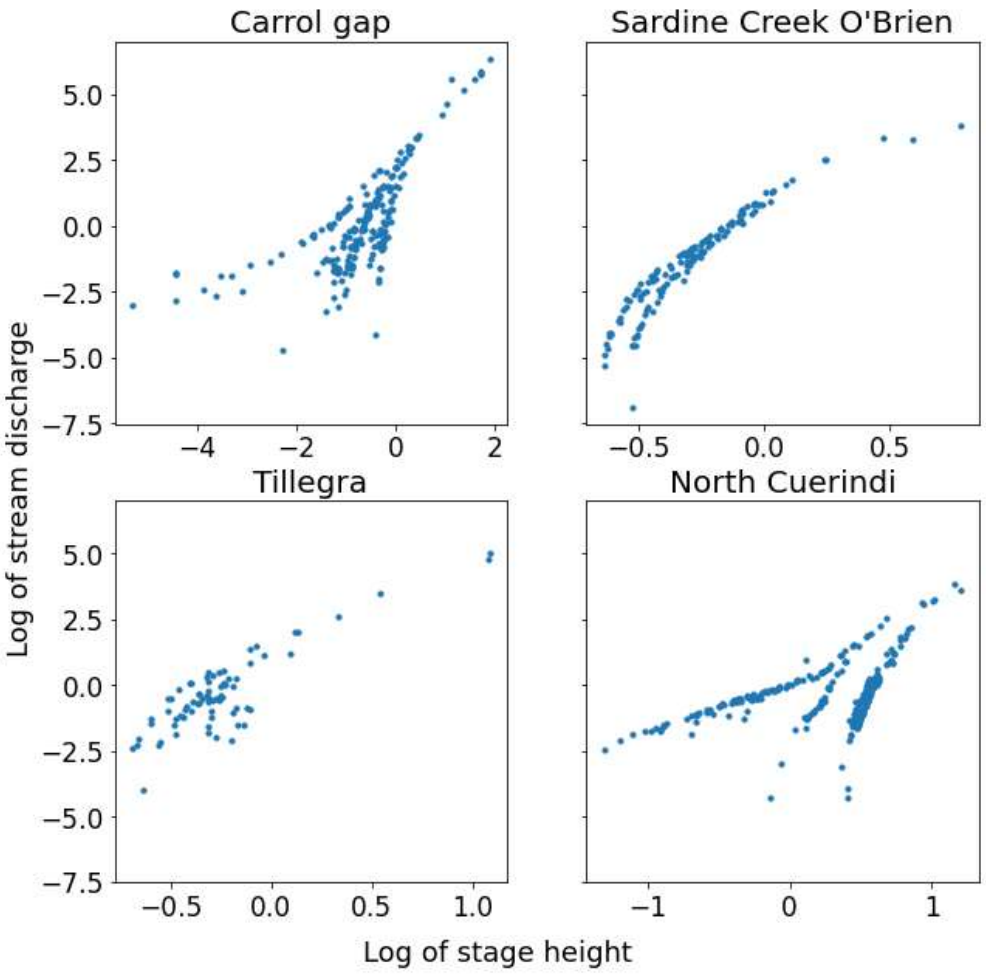

FIGURE 4.1. Streamflow gauging stations used in the study.
Top left: Carroll Gap; Top right: Sardine Creek O'Brien;
Bottom left: Tillegra; Bottom right: North Cuerindi

4.7 Results

4.7.1 Simulated data

4.7.1.1 Stationary rating curve estimation

This section demonstrates how the proposed AdaptRatin can be used to estimate the stage discharge relationship even when the true stage-discharge relationship is stationary and does

not change in time. To simulate data from a stationary stage-discharge relationship, data from the North Cuerindi station in Namoi river for the period 1950/1/1 - 1960/1/1 is used to generate the design matrix $\mathbf{X}$. Fifty random realizations of log discharge, $\mathbf{y}$, were generated using parameter values close to the true posterior mean of the parameters obtained when estimating the stage-discharge relationship for the dataset using AdaptRatin by setting $m_{\text{max}} = 1$.

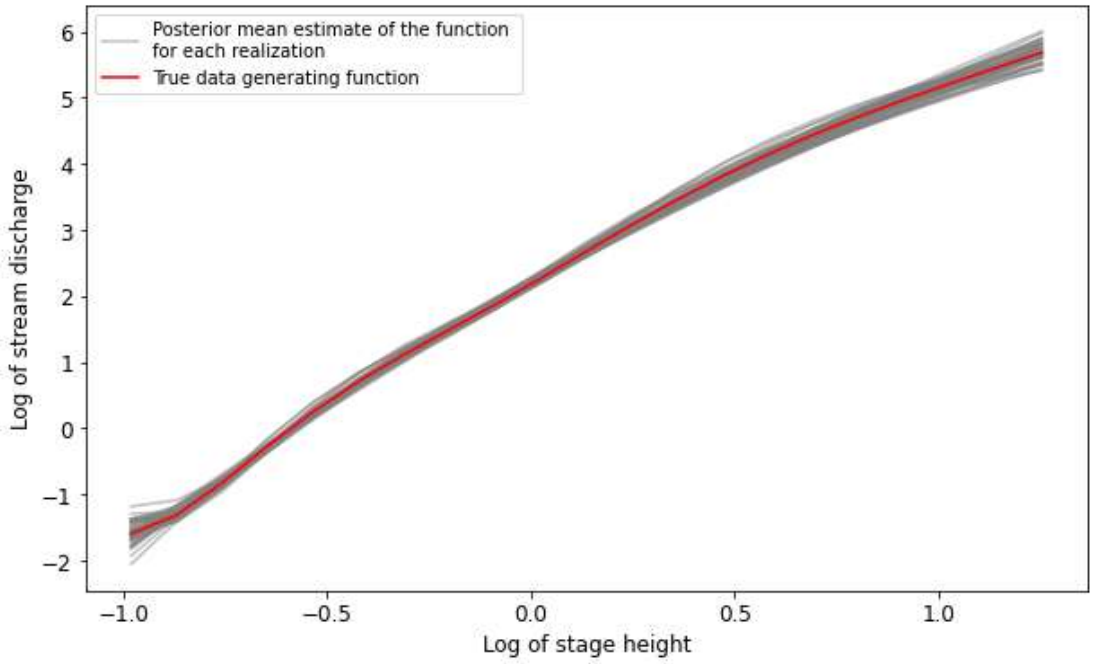

FIGURE 4.2. Posterior mean estimates of the functions for each relaization

Figure 4.2 depicts the data generating function (red) alongside the posterior mean estimates of the functions derived for each realization (grey). The posterior estimate $\widehat{Pr}(m = 1|\mathcal{G})$ serves as an estimation of the probability that the stage-discharge relationship remains stationary, while $\widehat{Pr}(m > 1|\mathcal{G})$ denotes the probability of deviations from stationarity. For the entire simulation, the maximum value obtained for $\widehat{Pr}(m > 1|\mathcal{G})$ was 0.002 while the mean for the estimate $\widehat{Pr}(m = 1|\mathcal{G})$ was 0.99. This indicates that AdaptRatin will not segment the data when the true stage-discharge relationship is indeed stationary.

4.7.1.2 Frequentist properties of the segmentation

In this section, the focus is on AdaptRatin's ability to correctly segment the gauging data into separate stationary periods. This includes the ability to estimate the number of segments and the locations of the partition points. Real gauging data from the North Cuerindi station in Namoi river for the period 1990/1/1 - 2008/1/1 is used to generate the design matrix $\mathbf{X}$. This station and the period was specifically chosen as it presents an example of a clear shift in the rating curve and an instance where the rating curves overlap as seen in Figure 4.3. Fifty random realizations of log stream discharge, $\mathbf{y}$, were generated using parameter values close to the true posterior mean of the parameters obtained when estimating the stage-discharge relationship for the dataset using AdaptRatin by setting $m_{\text{min}} = m_{\text{max}} = 3$.

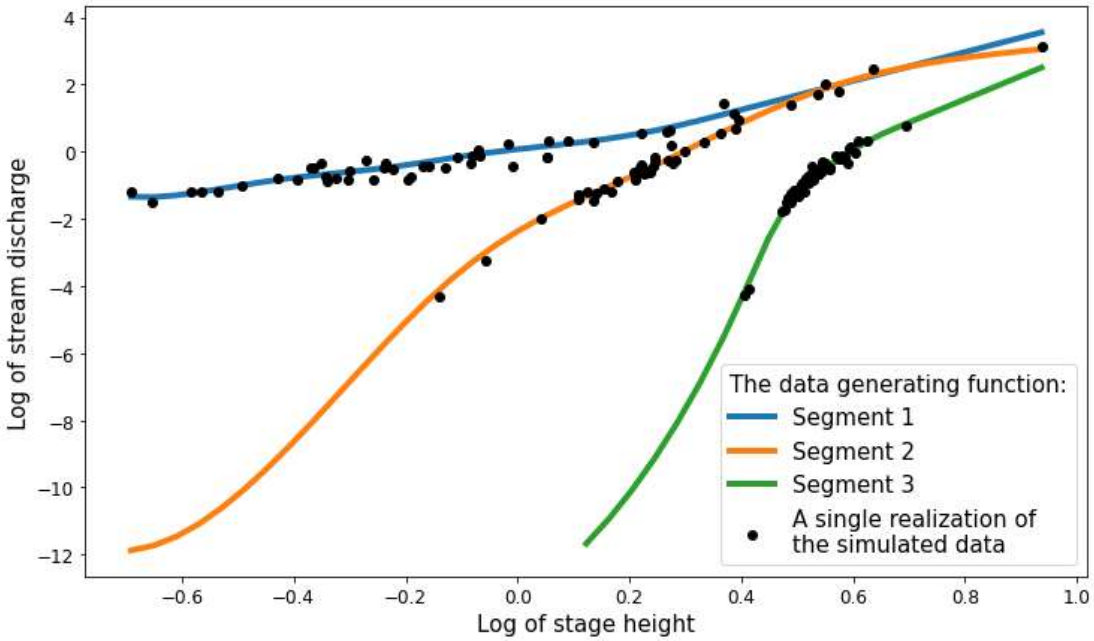

FIGURE 4.3. The data generating functions along with a single realization of the simulated data

During the estimation process for each of the 50 random realizations, m_{min} is set to 1 and m_{max} is set to 10.

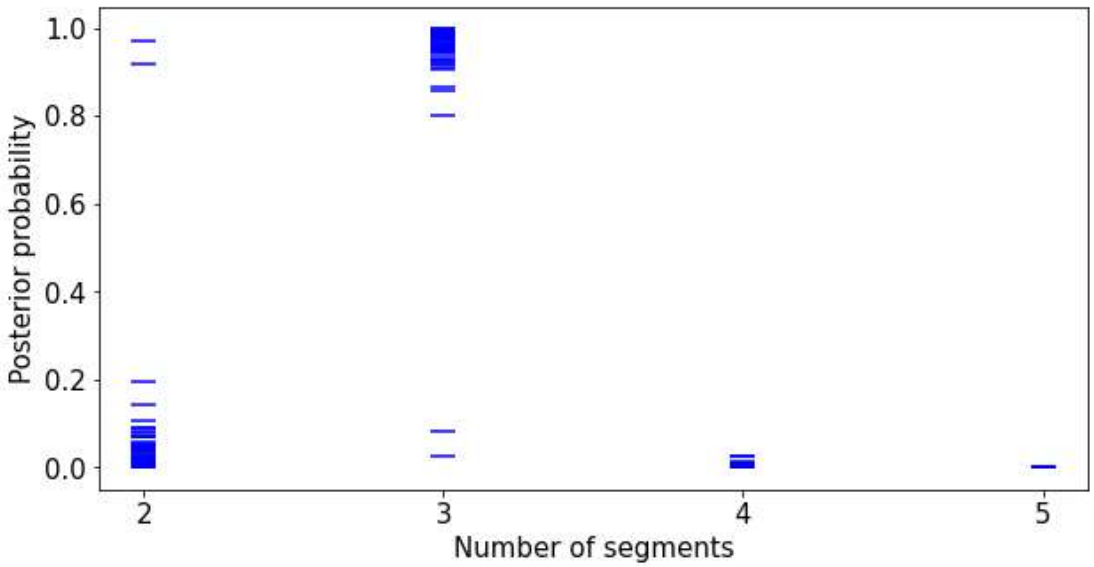

FIGURE 4.4. Posterior probability of the number of segments for each of the 50 random realizations

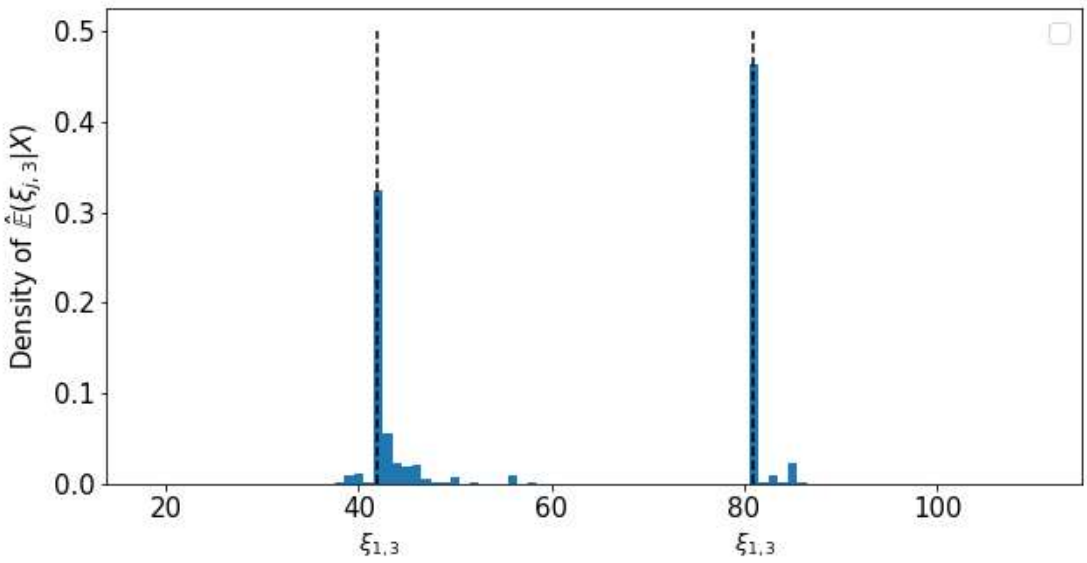

FIGURE 4.5. Density histogram of the posterior means of the partition points with $m = 3$, for the 50 random realizations. The dashed vertical line denotes the true partition points used to generate the data

Figure 4.4 presents the posterior probability of the number of segments for each of the 50 random realizations. The posterior probability $\widehat{Pr}(m = 3|\mathcal{G})$ is close to 0.9 for most of the 50 estimations. Figure 4.5 shows the density histograms of the estimated posterior means of the partition points $\hat{E}(\xi_{j,3})$ for $j = 1, 2$. It is evident that AdaptRatin has correctly located the partition points for each stationary rating curve period. Furthermore, the level of uncertainty in the predicted partition point $\xi_{2,3}$ is considerably less than that of $\xi_{1,3}$. This is as expected since the data generating functions used for the segments 2 and 3 are far apart from each other compared to segment 1 and 2 as seen in Figure 4.3

4.7.2 Real data

In this section, results from AdaptRatin for three gauging stations are presented. For each dataset, i_{min} is set to ten, ensuring that at least ten gaugings are needed to estimate a stationary rating curve. Although this number can be reduced, it is not recommended because doing so would significantly impact the accuracy of the rating curve estimation due to insufficient data. Only the rating curve estimate for each segment within the range of the available gauging data is displayed without extrapolation. When data is unavailable, extrapolation using the proposed method would result in estimates with high levels of uncertainty. This issue related to extrapolation and possible remedies are further discussed in section 4.8.

4.7.2.1 Carrol Gap

Carroll Gap station in Peel river had the most rating curve changes out of the three stations studied in this chapter. Table 4.2 reports the posterior probability of the number of segments while Figure 4.6 shows the predicted segmentation from AdaptRatin using the posterior mode of $\xi_{m=6}$. Figure 4.7 shows how AdaptRatin segments the time ordered gauging data and predicts the underlying stage-discharge relationship for each segment.

TABLE 4.2. Posterior probability of the number of segments: Carroll Gap station

Number of segments m	Posterior probability $\widehat{Pr}(m = k\|\mathcal{G})$
6	0.73
7	0.23
8	0.03
9	0.01

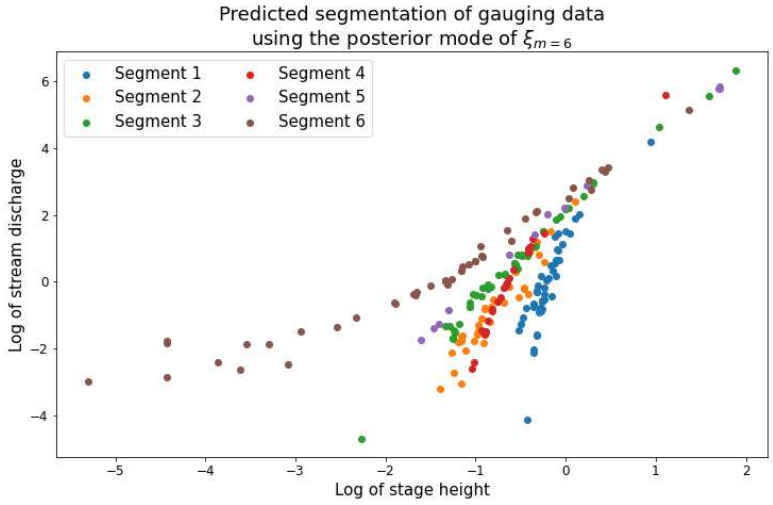

FIGURE 4.6. Predicted segmentation of the gauging data using the posterior mode of $\xi_{m=6}$

Figure 4.8 shows the uncertainty related to each partition point for the Carroll Gap station gauging data. The partition points $\xi_{3,6}, \xi_{4,6}$ and $\xi_{5,6}$ have a lower uncertainty compared to $\xi_{1,6}$ and $\xi_{2,6}$. This observation can be interpreted by visually inspecting the corresponding gauging data for each segment in Figure 4.6. The separation between the gauging data for segments 5-6 (purple and brown), 4-5 (red and purple) and 3-4 (green and red) is greater than that of segments 1-2 (blue and orange) and 2-3 (orange and green).

The posterior predictive mean rating curve along with the 95% credible intervals are plotted for each segment in Figure 4.9. The estimated rating curves for segments 1 and 2 in Figure 4.9 may have missed a possible additional segment and this might explain the higher level of uncertainty observed in the partition point between segments 1-2 and 2-3 explained before

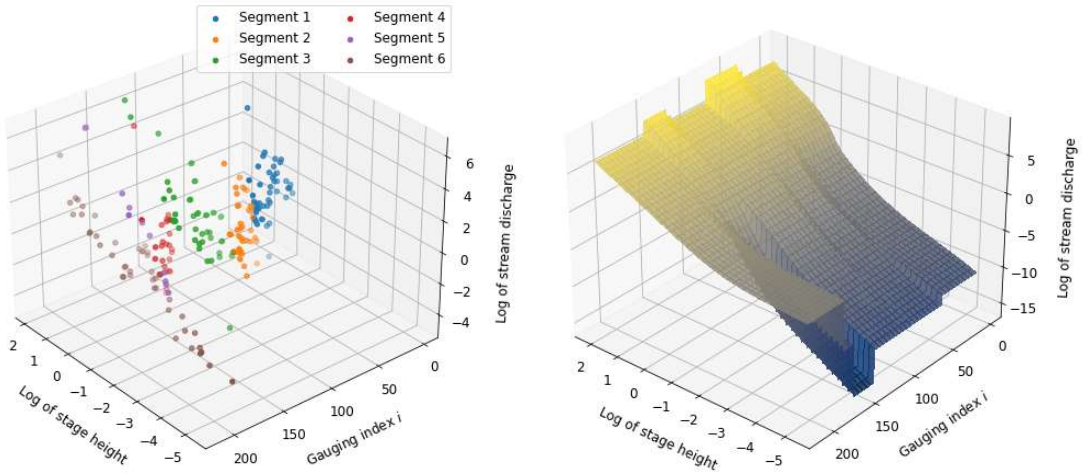

(A) AdaptRatin segmented gauging data

(B) Predicted stage-discharge relationship across time using AdaptRatin

FIGURE 4.7. The segmentation of the gauging data using AdaptRatin (on left) and the predicted non-stationary stage-discharge relationship using AdaptRatin (on right)

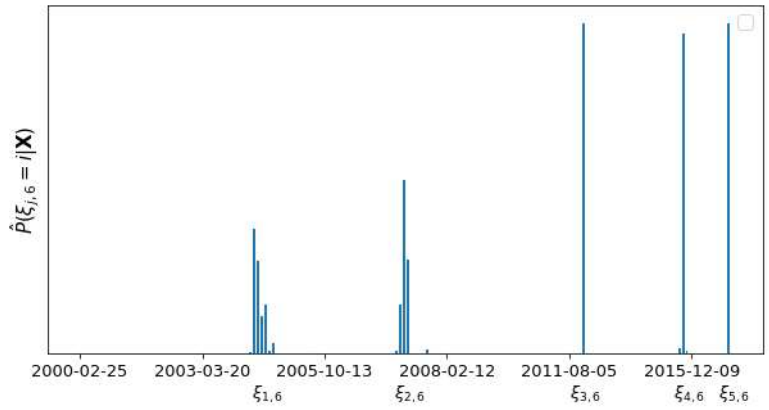

FIGURE 4.8. Posterior probability of the partition points $\xi_{j,6} = i$ for the Carroll Gap station data

in Figure 4.8. One reason could be due to the restriction on $i_{\min}$ value that was assigned in the sampling scheme. It is also worth noting the posterior probability of $\widehat{Pr}(m = 7|\mathcal{G})$ which was 0.23 indicating a possibility for an additional segment. The posterior mode of $\xi_{2,m=7}$ suggests this additional partition point to be on segment 2.

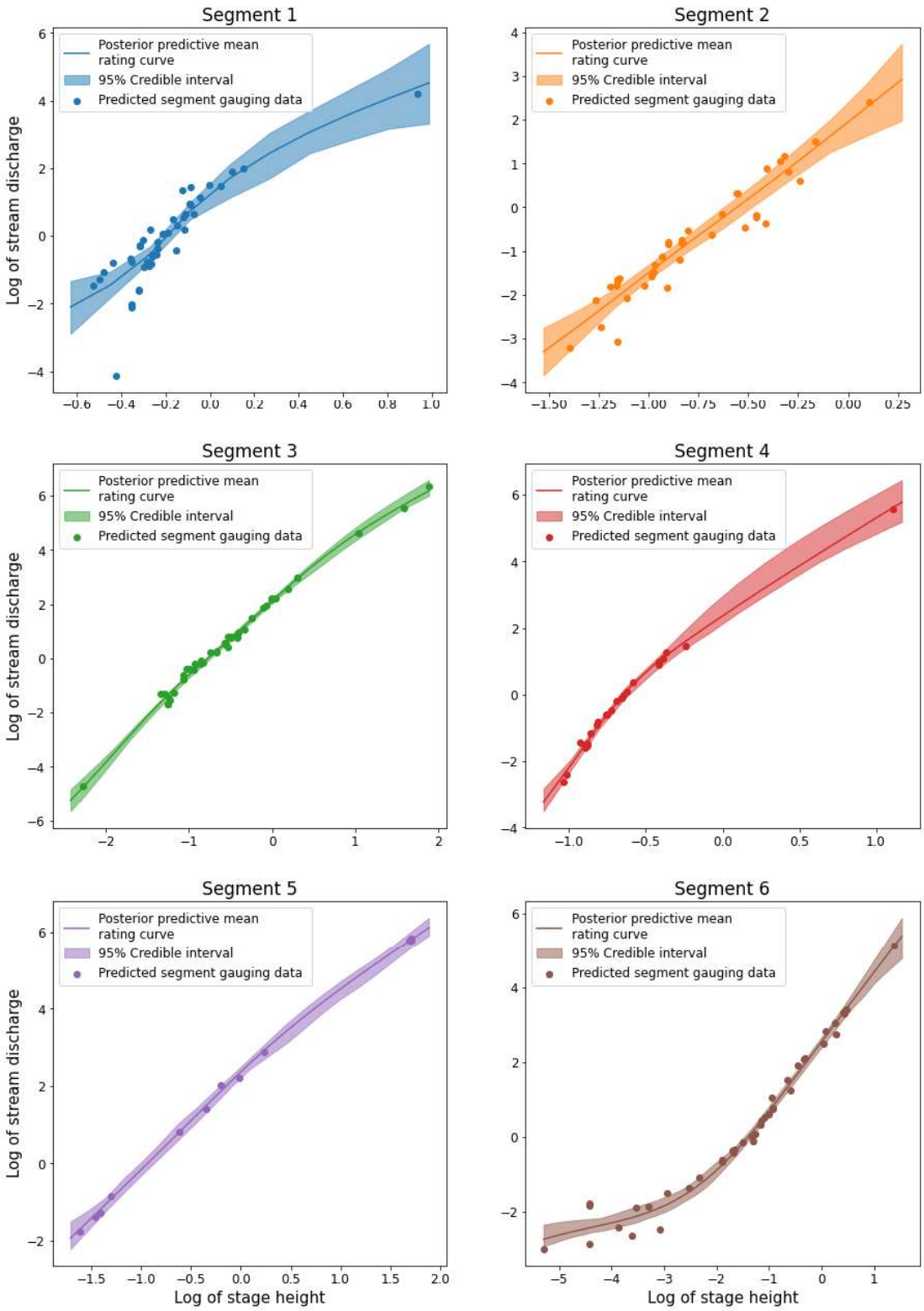

FIGURE 4.9. Posterior predictive mean rating curves for the six segments predicted using AdaptRatin for the Carroll Gap station in Peel river.

4.7.2.2 Sardine Creek O'Brien

This section presents the results from AdaptRatin for the Sardine Creek O'Brien station in Lerderderg river. The gauging data from this station had the lowest variability compared to the other stations considered in this study.

Table 4.3 presents the posterior probability of the number of segments while Figure 4.10 shows the predicted segmentation from AdaptRatin using the posterior mode of $\xi_{m=2}$.

TABLE 4.3. Posterior probability of the number of segments: Sardine Creek O'Brien

Number of segments m	Posterior probability $\widehat{Pr}(m = k\|\mathcal{G})$
2	0.83
3	0.17

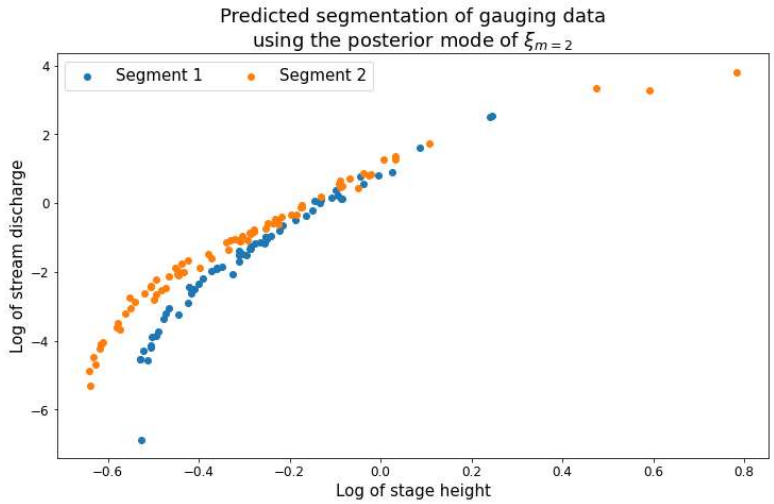

FIGURE 4.10. Predicted segmentation of the gauging data using the posterior mode of $\xi_{m=2}$

The posterior predictive mean rating curve along with the 95% credible intervals are plotted for the two segments in Figure 4.11.

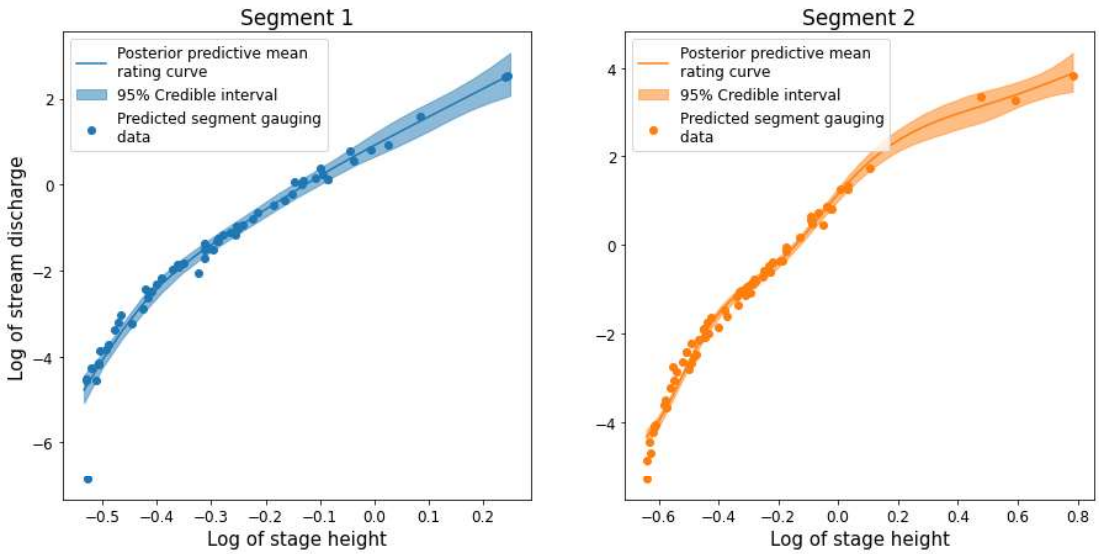

FIGURE 4.11. Posterior predictive mean rating curves for the six segments predicted using AdaptRatin for the Sardine Creek O'Brien station in Lerderberg river.

4.7.2.3 Tillegra

This section presents the results from AdaptRatin for the data from Tillegra station in William river. Gauging data for a shorter period of time was used from this station to assess how AdaptRatin performs with limited gauging data.

Table 4.4 reports the posterior probability of the number of segments while Figure 4.12 shows the predicted segmentation from AdaptRatin using the posterior mode of $\xi_{m=4}$

TABLE 4.4. Posterior probability of the number of segments Tillegra station

Number of segments m	Posterior probability $\widehat{Pr}(m = k\|\mathcal{G})$
4	0.81
5	0.16
6	0.03

The posterior predictive mean rating curve along with the 95% credible intervals are plotted for the four segments in Figure 4.13.

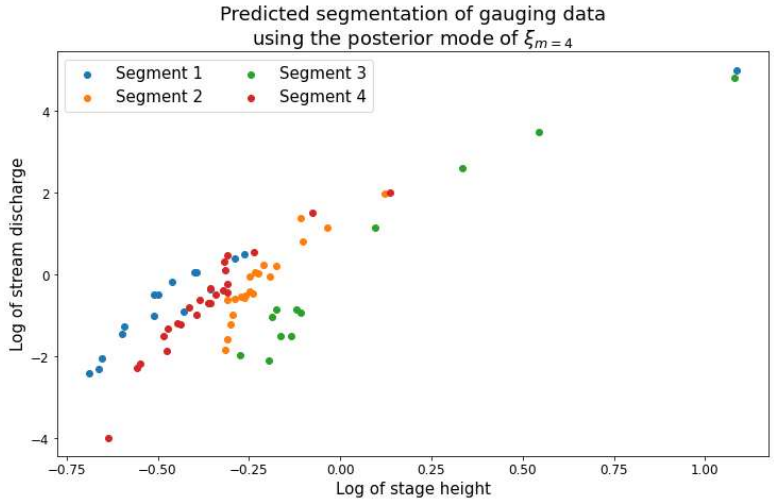

FIGURE 4.12. Predicted segmentation of the gauging data using the posterior mode of $\xi_{m=4}$

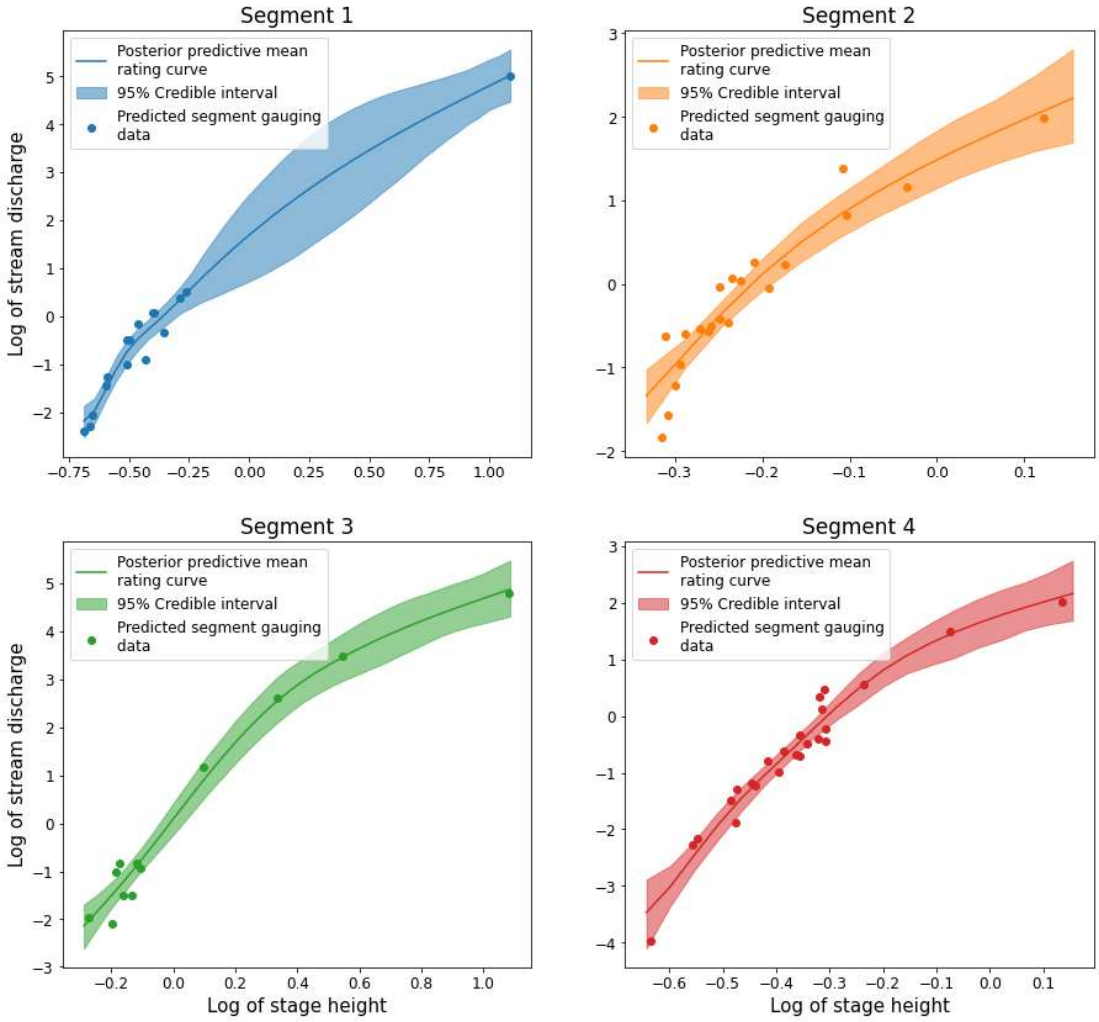

FIGURE 4.13. Posterior predictive mean rating curves for the four segments predicted using AdaptRatin for the Tillegra station in William river.

4.7.3 Comparison with BOM rating curve estimates

In this section, the estimated rating curves using AdaptRatin are compared with the rating curves published[1] by the Bureau of Meteorology (which are referred to as BOM estimates), for the three stations.

For all three stations (Figure 4.14: Carroll Gap station; Figure 4.15: Tillegra station, Figure 4.16: Sardine Creek at O'Brien station), the estimated rating curve for each stationary period predicted using AdaptRatin is plotted along with all the ratings published by the Bureau of Meteorology during the same period.

Analysing the estimated rating curve from AdaptRatin and the BOM estimates, for the period 2001/1/31 - 2004/5/20 for Carroll Gap station (top left panel of Figure 4.14), it is evident that AdaptRatin has missed an additional segment as explained previously in section 4.7.2.1. It is also worth noting how the BOM estimates have been extrapolated beyond the range of the gaugings for all the periods and some have estimates which do not agree with any of the gaugings available for these periods (see BOM estimates for the periods: 2004/5/21 - 2007/8/16, 2007/8/17 - 2011/11/3, 2011/11/4 - 2015/6/25 and 2016/11/9 - 2023). A similar observation can be seen for the BOM estimates for the Tillegra station as well (Figure 4.15, see BOM estimates for the periods: 2007/11/14 - 2013/1/17, 2013/1/18 - 2016/1/7 and 2016/1/8 - 2023/1/1). Such extrapolation and rating estimates without gauging data from the Bureau of Meteorology could be based on prior hydrological expert knowledge and hence AdaptRatin which is a data driven approach will not be able to recover those.

[1]The rating curves published by the Bureau of Meteorology are taken from http://www.bom.gov.au/waterdata/

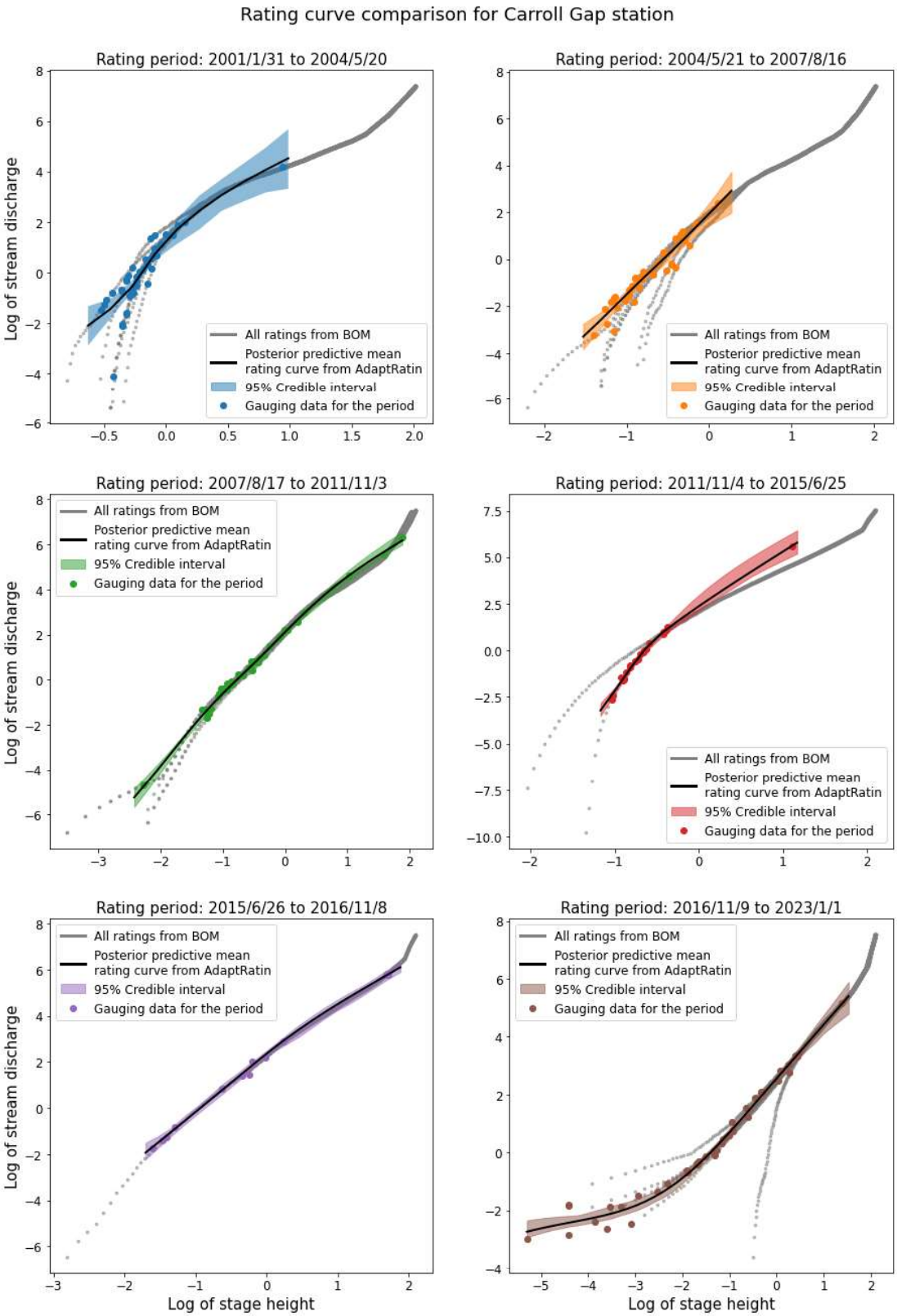

FIGURE 4.14. Plot of estimated rating curves for each stationary period predicted using AdaptRatin along with all the ratings published by the Bureau of Meteorology during the same period (in grey) for Carroll Gap station

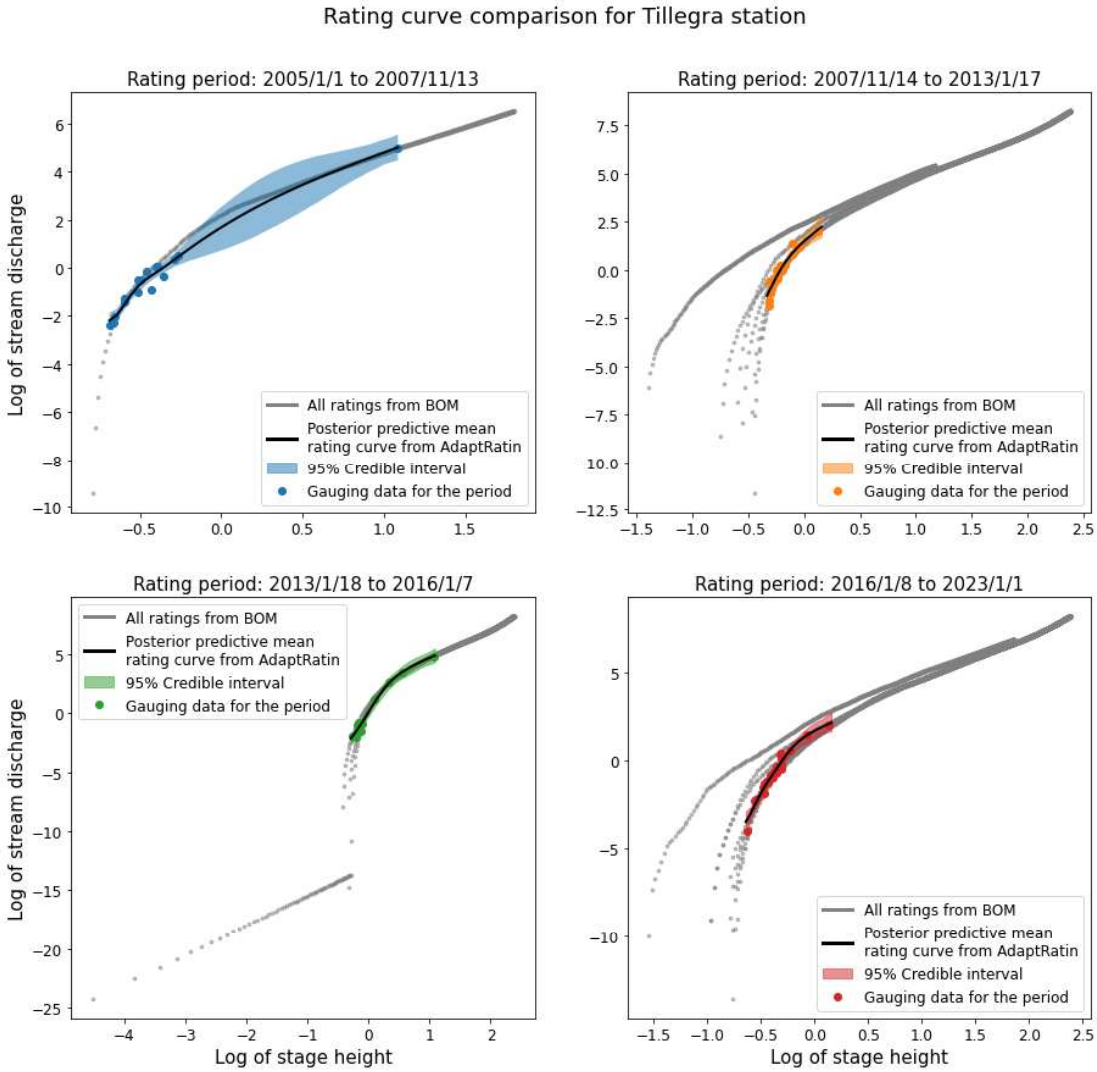

FIGURE 4.15. Plot of estimated rating curves for each stationary period predicted using AdaptRatin along with all the ratings published by the Bureau of Meteorology during the same period (in grey) for Tillegra station

The AdaptRatin estimates for the Sardine Creek O'Brien station given in Figure 4.16 have a better agreement with the BOM estimates than the Carroll Gap and Tillegra stations. The extrapolation of the BOM estimates beyond the available gauging data is evident for this station as well.

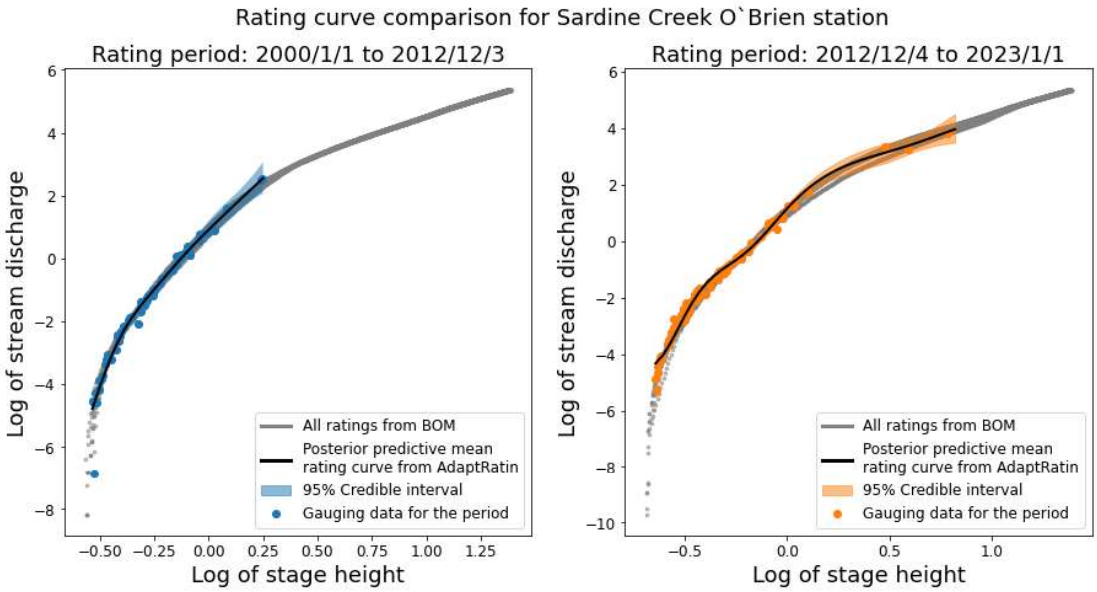

FIGURE 4.16. Plot of estimated rating curves for each stationary period predicted using AdaptRatin along with all the ratings published by the Bureau of Meteorology during the same period (in grey) for Sardine Creek O'Brien station

4.8 Discussion

In this chapter of the thesis, the AdaptRatin method is introduced which can estimate the time varying stage-discharge relationship, formally known as the rating curve in hydrology. The proposed method is tested on three gauging stations in Australia which have distinct rating curve shapes and the results demonstrate how AdaptRatin can successfully capture the changes in the rating curve over time and provide reliable estimates of the underlying stage-discharge relationship for each time period.

Analysing the predicted change points using AdaptRatin with continuous stage height records can provide some insight into the causation of these rating curve shifts. Figures 4.17 and 4.18 shows the continuous stage-height record along with the predicted change points (given in red) using AdaptRatin for the Carroll Gap and Tillegra stations respectively. All the rating curve changes predicted using AdaptRatin have occurred around high stream height

events. However, not all the high stream height events have caused rating curve shifts and therefore supplementary information such as flood heights, debris flows and vegetation growth should be sought to determine the specific causation for each rating curve change. It is important to note that the focus of AdaptRatin is to identify the changes in the rating curve using gauging data and not to explore the causal mechanisms of these changes.

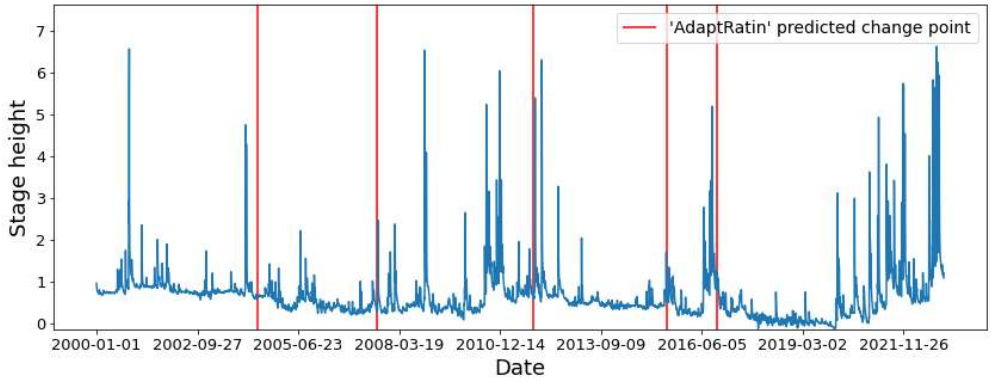

FIGURE 4.17. Plot of daily mean stage height for the Carroll Gap station. The predicted change points using AdaptRatin are given in red.

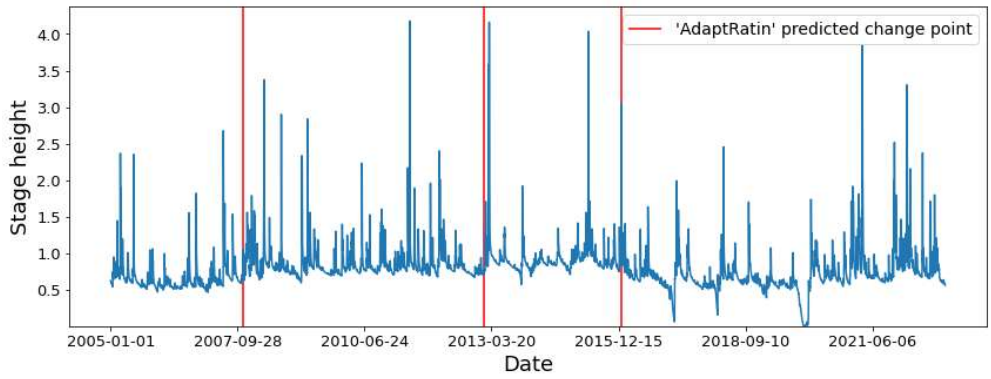

FIGURE 4.18. Plot of daily mean stage height for the Tillegra station. The predicted change points using AdaptRatin are given in red.

In the case of the Sardine Creek O'Brien station (Figure 4.19), the need for more frequent gauging is highlighted. If frequent gauging data is not available, the time taken to detect a change in the stage-discharge relationship will be longer leading to significant errors when

converting stage-heights to stream-discharge. Using an alternative approach to detect the exact timing of the rating curve change (Darienzo et al., 2021) instead of the gauging date when the rating curve has changed can potentially mitigate this issue. However, when no other information is available between gauging dates, any day between consecutive gauging dates is equally likely to be the exact change point and therefore this study does not interpolate between these gauging dates.

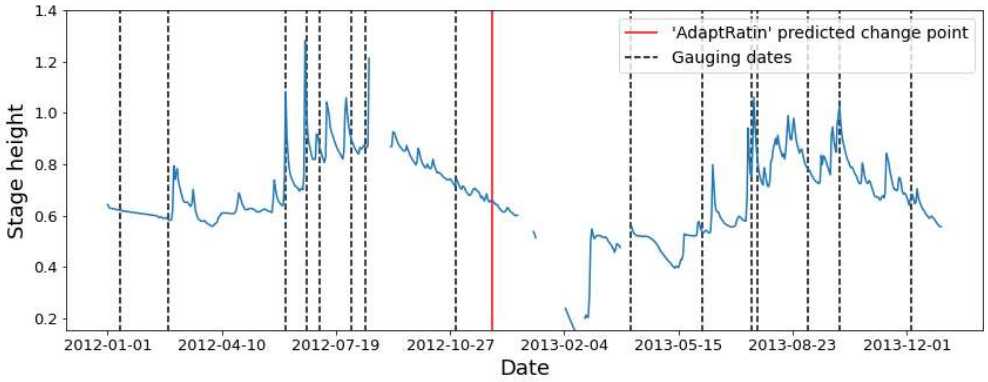

FIGURE 4.19. Plot of daily mean stage for the Sardine Creek O'Brien station. The predicted change point using AdaptRatin is given in red and the gauging dates are given in black dashed lines.

The estimated rating curves using AdaptRatin and the BOM estimates for the Sardine Creek O'Brien station are similar (Figure 4.16). However, several BOM estimates for the Carroll Gap and Tillegra stations (Figures 4.14 and 4.15 respectively) are found to deviate from the real gauging data and the estimates using AdaptRatin possibly due to these rating curves being generated purely from hydrological expert knowledge with no gauging data. The current version of AdaptRatin does not take any prior information about the shape of the rating curve (except that the rating curve has to be monotonically increasing) and relies on the gauging data to inform the shape of the station specific rating curve for each stationary period. Incorporating prior knowledge about the shape of the rating curve specifically to extrapolate where no gauging data is available (for example, high stage height gaugings) using supplementary data sources like remote sensing (Pham et al., 2021) could be a useful future research direction.

A limitation of the current AdaptRatin method is the requirement to specify a minimum number of gaugings for a valid segment i_{min} which can lead to some potential stationary periods to be missed like in the case of the first segment in Carroll Gap station if the available number of gaugings are less than i_{min} for the particular stationary period (Figure 4.9). Setting a smaller value for i_{min} could lead to poor estimates of the stage-discharge relationship and thus re-iterates the importance of having frequent gauging dates for stations which are known to have unstable rating curves. Improving AdaptRatin to assign i_{min} adaptively is another interesting future research direction.

4.9 Conclusion

Given the critical role of the rating curve in converting stage height measurements to stream discharge estimates, this chapter of the thesis proposes the Adaptive Streamflow Rating Curve Estimation (AdaptRatin) method which is reproducible and can be easily automated, to estimate the non-stationary stage-discharge relationship. AdaptRatin segments the time series into an unknown yet finite number of segments and models the relationship between stage height and stream discharge by placing a Gaussian process prior over the unknown relationship. The results from the three gauging stations tested in this chapter indicate that AdaptRatin can identify sudden changes in the rating curve and provide reliable estimates of the underlying stage-discharge relationship. A major advantage of AdaptRatin as a data-driven approach is its ability to detect sudden changes with minimal prior information while also providing measures of uncertainty about the change points, setting it apart from other currently available methods.

Appendix D (Chapter 4): Derived conditional posterior distributions of the parameters in AdaptRatin

The conditional posterior distributions of the parameters α, β, σ^2 and τ^2 are used as proposal distributions in the sampling algorithm explained in Appendix E.

$$\begin{aligned} p(\boldsymbol{\alpha}|\mathbf{y}, \mathbf{X}, \boldsymbol{\beta}, \sigma^2) &\sim \mathcal{N}(\boldsymbol{\mu}_\alpha, \boldsymbol{\Lambda}_\alpha^{-1}) \\ \boldsymbol{\mu}_\alpha &= \boldsymbol{\Lambda}_\alpha^{-1}\mathbf{X}'\boldsymbol{\Sigma}_y^{-1}(\mathbf{y} - \mathbf{V}\boldsymbol{\beta}) \\ \boldsymbol{\Lambda}_\alpha &= \mathbf{X}'\boldsymbol{\Sigma}_y^{-1}\mathbf{X} + \boldsymbol{\Sigma}_\alpha^{-1} \\ \boldsymbol{\Sigma}_y &= \sigma^2\mathbf{I_n} \\ \boldsymbol{\Sigma}_\alpha &= c_\alpha\mathbf{I}_2 \end{aligned} \tag{.2}$$

$$\begin{aligned} p(\boldsymbol{\beta}|\mathbf{y}, \mathbf{X}, \sigma^2, \boldsymbol{\alpha}, \tau^2) &\sim \mathcal{N}(\boldsymbol{\mu}_\beta, \boldsymbol{\Lambda}_\beta^{-1}) \\ \boldsymbol{\mu}_\beta &= \boldsymbol{\Lambda}_\beta^{-1}\mathbf{V}'\boldsymbol{\Sigma}_y^{-1}(\mathbf{y} - \mathbf{X}\boldsymbol{\alpha}) \\ \boldsymbol{\Lambda}_\beta &= \mathbf{V}'\boldsymbol{\Sigma}_y^{-1}\mathbf{V} + \boldsymbol{\Sigma}_\beta^{-1} \\ \boldsymbol{\Sigma}_\beta &= \tau^2\boldsymbol{\lambda} \end{aligned} \tag{.3}$$

$$\begin{aligned} p(\boldsymbol{\sigma}^2|\mathbf{y}, \mathbf{X}, \boldsymbol{\beta}, \boldsymbol{\alpha}) &\sim \mathcal{IG}(u^*, v^*) \\ u^* &= \frac{n}{2} + u_0 \\ v^* &= \frac{1}{2}\left((\mathbf{y} - (\mathbf{X}\boldsymbol{\alpha} + \mathbf{V}\boldsymbol{\beta}))'(\mathbf{y} - (\mathbf{X}\boldsymbol{\alpha} + \mathbf{V}\boldsymbol{\beta})) + 2v_0\right) \end{aligned} \tag{.4}$$

$$\begin{aligned} p(\boldsymbol{\tau}^2|\boldsymbol{\beta}) &\sim \mathcal{IG}(a^*, b^*) \\ a^* &= \frac{n}{2} + a_0 \\ b^* &= \frac{1}{2}\left(\boldsymbol{\beta}'\boldsymbol{\lambda}^{-1}\boldsymbol{\beta} + 2b_0\right) \end{aligned} \tag{.5}$$

Appendix E (Chapter 4): Sampling algorithm

This section provides the detailed sampling algorithm specific to AdaptRatin introduced in chapter 4 of this thesis which is based on AdaptSPEC (Rosen et al., 2012).

Within model moves

Assuming the chain is at $\Psi^c := (\boldsymbol{\beta}^c, \boldsymbol{\sigma}^{2p}, \xi^c, \boldsymbol{\tau}^{2c})$, it is suggested that the transition to $\Psi^p := (\boldsymbol{\beta}^p, \boldsymbol{\sigma}^{2p}, \xi^p, \boldsymbol{\tau}^{2p})$ be made according to the following procedure:

(1) First, a segment boundary j is selected to relocate from the $m-1$ available options with equal probability of choosing any segment boundary.

$$Pr(j = k^*) := (m-1)^{-1}$$

(2) Then a segment boundary $\xi^p_{k^*}$ is chosen from the interval $[\xi^c_{k^*-1}, \xi^c_{k^*+1}]$, subject to the constraint that each affected segment satisfies the minimum number of data points for a valid segment. So that the complete move is ,

$$Pr(\xi^p_{k^*} = i) := Pr(j = k^*) \times Pr(\xi^p_{k^*} = i | j = k^*)$$

(3) To explore the parameter space efficiently, a mixture distribution is constructed for $Pr(\xi^p_{k^*} = i|j = k^*)$ so that,

$$Pr(\xi^p_{k^*} = i|j = k^*) := \pi q_{\xi_1}(\xi^p_{k^*} = i|\xi^c_{k^*}) + (1-\pi) q_{\xi_2}(\xi^p_{k^*} = i|\xi^c_{k^*}),$$

where $q_{\xi_1}(\xi^p_{k^*} = i|\xi^c_{k^*}) := (n_{k^*} + n_{k^*+1} - 2i_{\min} + 1)^{-1}$

$$q_{\xi_2}(\xi^p_{k^*} = i|\xi^c_{k^*}) = \begin{cases} 0 & \text{if } |i - \xi^c_{k^*}| > 1 \\ \frac{1}{3} & \text{if } |i - \xi^c_{k^*}| \leq 1, n_{k^*} \neq i_{\text{min}} \text{ and } n_{k^*+1} \neq i_{\text{min}} \\ \frac{1}{2} & \text{if } i - \xi^c_{k^*} \leq 1, n_{k^*} = i_{\text{min}} \text{ and } n_{k^*+1} \neq i_{\text{min}} \\ \frac{1}{2} & \text{if } \xi^c_{k^*} - i \leq 1, n_{k^*} \neq i_{\text{min}} \text{ and } n_{k^*+1} = i_{\text{min}} \\ 1 & \text{if } i = \xi^c_{k^*}, n_{k^*} = i_{\text{min}} \text{ and } n_{k^*+1} = i_{\text{min}} \end{cases}$$

The support of q_1 and q_2 reveals their distinct characteristics: q_1, spanning $n_{k^*} + n_{k^*+1} - (2 \times i_{min}) + 1$ data points, facilitates larger jumps, whereas q_2, covering a maximum of 3 data points, enables smaller steps, thereby enhancing the acceptance rate. As given in Rosen et al. (2012), combining these two proposals with a mixture weight π of 0.2 is found to achieve a favorable balance between swift exploration of the parameter space and a satisfactory acceptance rate.

(4) After proposing the new segment boundaries, $\xi^p_{k^*}$, the rating curve parameters for the two segments $j = k^*, k^* + 1$ impacted by the boundary adjustment are updated. Let $\alpha^p_* := (\boldsymbol{\alpha}^p_{k^*}, \boldsymbol{\alpha}^p_{k^*+1})'$, $\boldsymbol{\beta}^p_* := (\boldsymbol{\beta}^p_{k^*}, \boldsymbol{\beta}^p_{k^*+1})'$ and $\boldsymbol{\sigma}^{2p}_* := (\sigma^{2p}_{k^*}, \sigma^{2p}_{k^*+1})'$ be the parameters to be updated which are drawn from the proposal densities given by Equations .2, .3 and .4 respectively in sequence.

(5) The proposal densities evaluated at $\boldsymbol{\alpha}^p_*$, $\boldsymbol{\beta}^p_*$, and $\boldsymbol{\sigma}^{2p}_*$, for $j = k^*, k^* + 1$ are

$$q_\alpha(\boldsymbol{\alpha}^p_*|\mathbf{X}^p_*, \mathbf{y}^p_*, \boldsymbol{\beta}^c_*, \boldsymbol{\sigma}^{2c}_*) := \prod_{j=k^*}^{k^*+1} q(\boldsymbol{\alpha}^p_j|\mathbf{X}^p_j, \mathbf{y}^p_*, \boldsymbol{\beta}^c_j, \boldsymbol{\sigma}^{2c}_j),$$

$$q_\beta(\boldsymbol{\beta}^p_*|\mathbf{X}^p_*, \mathbf{y}^p_*, \boldsymbol{\alpha}^p_*, \boldsymbol{\sigma}^c_*, \boldsymbol{\tau}^2_*) := \prod_{j=k^*}^{k^*+1} q(\beta^{2p}_j|\mathbf{X}^p_j, \mathbf{y}^p_j, \boldsymbol{\alpha}^p_j, \boldsymbol{\sigma}^c_j, \tau^2_j),$$

$$q_\sigma(\boldsymbol{\sigma}^{2p}_*|\mathbf{X}^p_*, \mathbf{y}^p_*, \boldsymbol{\beta}^p_*, \boldsymbol{\alpha}^p_*) := \prod_{j=k^*}^{k^*+1} q(\sigma^{2p}_j|\mathbf{X}^p_j, \mathbf{y}^p_j, \boldsymbol{\alpha}^p_j, \boldsymbol{\beta}^p_j),$$

Similarly, the proposal densities at the current values of $\boldsymbol{\alpha}^c_*$, $\boldsymbol{\beta}^c_*$, and $\boldsymbol{\sigma}^{2c}_*$ are evaluated.

(6) Next the proposed functions $g(\mathbf{X}^p|\boldsymbol{\alpha}_*^p, \boldsymbol{\beta}_*^*, \boldsymbol{\sigma}_*^{2p})$ are checked for the monotonically increasing constraint,

$$p(g(\mathbf{X}^p|\boldsymbol{\alpha}_*^p, \boldsymbol{\beta}_*^*, \boldsymbol{\sigma}_*^{2p})) = \begin{cases} 1 & \text{if } g(\mathbf{X}^p|\boldsymbol{\alpha}_*^p, \boldsymbol{\beta}_*^*, \boldsymbol{\sigma}_*^{2p}) \text{ is monotonically increasing} \\ 0 & \text{otherwise} \end{cases}$$

(7) The proposed $\alpha_*^p, \beta_*^p, \boldsymbol{\sigma}_*^{2p}$ and ξ^p is accepted with probability A_{within}

$$\begin{aligned} A_{\text{within}} &= \min\{1, \eta_{\text{within}}\} \\ \eta_{\text{within}} =& \frac{p(\mathbf{y}_*^p|\boldsymbol{\alpha}_*^p, \boldsymbol{\beta}_*^p, \boldsymbol{\sigma}_*^{2p}, \xi^p, \tau_*^2)p(\boldsymbol{\alpha}_*^p)p(\boldsymbol{\beta}_*^p|\tau_*^2)p(\boldsymbol{\sigma}_*^{2p})p(\xi^p)p(g(\mathbf{X}^p|\boldsymbol{\alpha}_*^p, \boldsymbol{\beta}_*^*, \boldsymbol{\sigma}_*^{2p}))}{p(\mathbf{y}_*^c|\boldsymbol{\alpha}_*^c, \boldsymbol{\beta}_*^c, \boldsymbol{\sigma}_*^{2c}, \xi^c, \tau_*^2)p(\boldsymbol{\alpha}_*^c)p(\boldsymbol{\beta}_*^c|\tau_*^2)p(\boldsymbol{\sigma}_*^{2c})p(\xi^c)} \\ &\times \frac{q_\alpha(\boldsymbol{\alpha}_*^c|\boldsymbol{\beta}_*^p, \sigma_*^{2p}, \xi^c)q_\beta(\boldsymbol{\beta}_*^c|\boldsymbol{\alpha}_*^c, \tau_*^2, \sigma_*^{2p}, \xi^c)q_\sigma(\boldsymbol{\sigma}_*^{2c}|\boldsymbol{\beta}_*^c, \boldsymbol{\alpha}_*^c, \xi^c)}{q_\alpha(\boldsymbol{\alpha}_*^p|\boldsymbol{\beta}_*^c, \sigma_*^{2c}, \xi^p)q_\beta(\boldsymbol{\beta}_*^p|\boldsymbol{\alpha}_*^p, \tau_*^2, \sigma_*^{2c}, \xi^p)q_\sigma(\boldsymbol{\sigma}_*^{2p}|\boldsymbol{\beta}_*^p, \boldsymbol{\alpha}_*^p, \xi^p)} \end{aligned} \tag{.6}$$

(8) Then the smoothing parameters for the updated segments, $\boldsymbol{\tau}_*^{2p} := (\tau_{k^*}^p, \tau_{k^*+1}^p)$ are drawn using the conditional posterior distribution of τ^2 given by Equation .5 and accepted with probability 1.

Between model moves

For this type of move, there are 2 possible options.

(1) Increase the number of segments by one (Birth).

$$m^p = m^c + 1$$

(2) Reduce the number of segments by one (Death).

$$m^p = m_c - 1$$

First it is decided whether the step is a birth or a death by checking:

(1) If the current number of segment $m^c = 1$, then a birth is always proposed

(2) If $m_{2\,\text{min}}^c$, the available number of segments which can be split to result in two valid segments is zero or the current number of segments m_c have reached the maximum

allowed segments M, then there are no splittable segments so a death step is always proposed.

(3) If none of the above conditions are met, a death or a birth step is proposed with equal probability.

Next the parameters affected are updated depending on the type of move. Suppose a birth step is proposed. Then the parameter update follows:

(1) Select randomly a segment to split from the available $m^c_{2\,\text{min}}$ segments.

$$q(j = k^*|m^p, m^c, \xi^c_{m^c}) = \frac{1}{m^c_{2\,\text{min}}}$$

(2) Then select a splitting position so that it generates two valid segments.

$$q(\xi^p_{k^*,m^p} = i|j = k^*, m^p, m^c, \xi^c_{m^c}) = \frac{1}{n_{k^*,m^c} - 2i_{\text{min}} + 1}$$

(3) First propose the smoothing parameters, $\boldsymbol{\tau}^{2p}_* = (\tau^{2p}_{k^*,m^p}, \tau^{2p}_{k^*+1,m^p})$ by drawing $u_{\tau^2} \sim \mathcal{U}[0,1]$, and letting $\tau^{2p}_{k^*,m^p}$ and $\tau^{2p}_{k^*+1,m^p}$ be deterministic functions of u_{τ^2} and $\tau^{2c}_{k^*,m^c}$;

$$\tau^{2p}_{k^*,m^p} = \tau^{2c}_{k^*,m^c} \times \frac{u_{\tau^2}}{1 - u_{\tau^2}}$$

$$\tau^{2p}_{k^*+1,m^p} = \tau^{2c}_{k^*,m^c} \times \frac{1 - u_{\tau^2}}{u_{\tau^2}}$$

(4) Similarly, $\alpha^p_* = (\boldsymbol{\alpha}^p_{k^*}, \boldsymbol{\alpha}^p_{k^*+1})$ is proposed by drawing $u_{\alpha_0} \sim \mathcal{U}[-1,1]$ and $u_{\alpha_1} \sim \mathcal{U}[-1,1]$, and letting the intercept and slope (α_0 and α_1) be deterministic functions of u_{α_0} and α_{0,k^*,m^c}, and u_{α_1} and α_{1,k^*,m^c} respectively.

$$\begin{aligned}
\alpha_{0,k^*,m^p} &= \alpha_{0,k^*,m^c} + u_{\alpha_0} \\
\alpha_{0,k^*+1,m^p} &= \alpha_{0,k^*,m^c} - u_{\alpha_0} \\
\alpha_{\text{`},k^*,m^p} &= \alpha_{1,k^*,m^c} + u_{\alpha_1} \\
\alpha_{1,k^*+1,m^p} &= \alpha_{1,k^*,m^c} - u_{\alpha_1}
\end{aligned}$$

(5) Similarly, $\boldsymbol{\sigma}_*^{2p} = (\sigma^{2p}_{k^*,m^p}, \sigma^{2p}_{k^*+1,m^p})$ is proposed by drawing $u_{\sigma^2} \sim \mathcal{U}[0,1]$ and letting $\sigma^{2p}_{k^*,m^p}$ and $\sigma^{2p}_{k^*+1,m^p}$ be deterministic functions of u_{σ^2} and $\sigma^{2c}_{k^*,m^c}$

$$\sigma^{2p}_{k^*,m^p} = \sigma^{2c}_{k^*,m^c} \times \frac{u_{\sigma^2}}{1-u_{\sigma^2}}$$

$$\sigma^{2p}_{k^*+1,m^p} = \sigma^{2c}_{k^*,m^c} \times \frac{1-u_{\sigma^2}}{u_{\sigma^2}}$$

(6) Then $\boldsymbol{\beta}_*^p := (\boldsymbol{\beta}^p_{k^*}, \boldsymbol{\beta}^p_{k^*+1})$ is proposed from the density given in Equation .3

(7) Next the proposed functions $g(\mathbf{X}^p|\boldsymbol{\alpha}_*^p, \boldsymbol{\beta}_*^*, \boldsymbol{\sigma}_*^{2p})$ are checked for the monotonically increasing constraint,

$$p(g(\mathbf{X}^p|\boldsymbol{\alpha}_*^p, \boldsymbol{\beta}_*^*, \boldsymbol{\sigma}_*^{2p})) = \begin{cases} 1 & \text{if } g(\mathbf{X}^p|\boldsymbol{\alpha}_*^p, \boldsymbol{\beta}_*^*, \boldsymbol{\sigma}_*^{2p}) \text{ is monotonically increasing} \\ 0 & \text{otherwise} \end{cases}$$

(8) Finally, the proposed $\boldsymbol{\beta}_*^p, \boldsymbol{\alpha}_*^p, \boldsymbol{\sigma}_*^{2p}, \boldsymbol{\tau}_*^{2p}$ and the move $\xi^p_{m^p}$ are jointly accepted with probability A_{between}

$$A_{\text{between}} = \min\{1, \eta_b\}$$

$$\begin{aligned}
\eta_b = & \frac{p(\mathbf{y}|\boldsymbol{\alpha}_{m^p}, \boldsymbol{\sigma}^{2p}_{m^p}, \boldsymbol{\beta}_{m^p}, \boldsymbol{\tau}^2_{m^p}, \boldsymbol{\xi}^p_{m^p}) p(\boldsymbol{\alpha}_{m^p}) p(\boldsymbol{\sigma}^{2p}_{m^p}) p(\boldsymbol{\beta}_{m_p}|\boldsymbol{\tau}^{2p}_{m^p}) p(\xi^p_{m^p}|m^p) p(g(\mathbf{X}^p|\boldsymbol{\alpha}_*^p, \boldsymbol{\beta}_*^*, \boldsymbol{\sigma}_*^{2p}))}{p(\mathbf{y}|\boldsymbol{\alpha}_{m^c}, \boldsymbol{\sigma}^{2c}_{m^c}, \boldsymbol{\beta}_{m^c}, \boldsymbol{\tau}^2_{m^c}, \boldsymbol{\xi}^c_{m^c}) p(\boldsymbol{\alpha}_{m^c}) p(\boldsymbol{\sigma}^{2c}_{m^c}) p(\boldsymbol{\beta}_{m_c}|\boldsymbol{\tau}^{2c}_{m^c}) p(\xi^c_{m^c}|m^c)} \\
& \times \frac{q(m^c|m^p, \xi^p_{m^p})}{q(m^p|m^c, \xi^c_{m^c}) q(\xi^p_{m^p}|\xi^c_{m^c})} \\
& \times \frac{q_\beta(\boldsymbol{\beta}^c_{k^*,m^c}|\boldsymbol{\alpha}^c_{k^*,m^c}, \boldsymbol{\sigma}^{2c}_{k^*,m^c}, \boldsymbol{\tau}^{2c}_{k^*,m^c}, \boldsymbol{\xi}^c)}{q_\beta(\boldsymbol{\beta}^p_{k^*,m^p}|\boldsymbol{\alpha}^p_{k^*,m^p}, \boldsymbol{\sigma}^{2p}_{k^*,m^p}, \boldsymbol{\tau}^{2p}_{k^*,m^p}, \boldsymbol{\xi}^p) q_\beta(\boldsymbol{\beta}^p_{k^*+1,m^p}|\boldsymbol{\alpha}^p_{k^*+1,m^p}, \boldsymbol{\sigma}^{2p}_{k^*+1,m^p}, \boldsymbol{\tau}^{2p}_{k^*+1,m^p}, \boldsymbol{\xi}^p)} \\
& \times \left|\frac{\partial(\sigma^{2p}_{k^*,m^p}, \sigma^{2p}_{k^*+1,m^p})}{\partial(\sigma^{2c}_{k^*,m^c}, u_{\sigma^2})}\right| \times \left|\frac{\partial(\tau^{2p}_{k^*,m^p}, \tau^{2p}_{k^*+1,m^p})}{\partial(\tau^{2c}_{k^*,m^c}, u_{\tau^2})}\right| \times \left|\frac{\partial(\alpha_{0,k^*,m^p}, \alpha_{0,k^*+1,m^p}, \alpha_{1,k^*,m^p}, \alpha_{1,k^*+1,m^p})}{\partial(\alpha_{0,k^*,m^c}, u_{\alpha_0}, \alpha_{1,k^*,m^c}, u_{\alpha_1})}\right|
\end{aligned}$$

For a death step, the reverse of a birth step is performed;

(1) A new partition $\xi^p_{m^p}$ is proposed by selecting one of $m^c - 1$ segment boundaries with equal probability of selecting each current segment boundary to be removed. Let the segment boundary selected for removal be $j = k^*$

$$q(\xi^p_{m^p}|m^p, m^c, \xi^c_{m^c}) = \frac{1}{m^c - 1}$$

(2) A single smoothing parameter $\tau^{2p}_{k^*,m^p}$ is proposed using $\tau^{2c}_{k^*,m^c}$ and $\tau^{2c}_{k^*+1,m^c}$ by reversing the process in bullet point (3) in the birth step.

$$\tau^{2p}_{k^*,m^p} = \sqrt{\tau^{2c}_{k^*,m^c} \times \tau^{2c}_{k^*+1,m^c}}$$

(3) Similarly, the reverse process is performed to generate $\boldsymbol{\alpha}^p_{m^p}$ and $\sigma^{2p}_{m^p}$

(4) $\beta^p_{m^p}$ is proposed from the density given in Equation .3 given the proposed $\boldsymbol{\alpha}^p_{m^p}$ and $\sigma^{2p}_{m^p}$.

(5) Next the proposed functions $g(\mathbf{X}^p|\boldsymbol{\alpha}^p_*, \boldsymbol{\beta}^*_*, \boldsymbol{\sigma}^{2p}_*)$ are checked for the monotonically increasing constraint,

$$p(g(\mathbf{X}^p|\boldsymbol{\alpha}^p_*, \boldsymbol{\beta}^*_*, \boldsymbol{\sigma}^{2p}_*)) = \begin{cases} 1 & \text{if } g(\mathbf{X}^p|\boldsymbol{\alpha}^p_*, \boldsymbol{\beta}^*_*, \boldsymbol{\sigma}^{2p}_*) \text{ is monotonically increasing} \\ 0 & \text{otherwise} \end{cases}$$

(6) The acceptance probability of the death step is the inverse of the acceptance probability of the birth step given in (.6).